Available online at www.sciencedirect.com
SCIENCE DIRECT®
Journal of Computational Physics 195 (2004) 655–676
JOURNAL OF COMPUTATIONAL PHYSICS
www.elsevier.com/locate/jcp

A generalized hydrodynamic computational model for rarefied and microscale diatomic gas flows

R.S. Myong *

Division of Mechanical and Aerospace Engineering and ReCAPT, Gyeongsang National University, Chinju, Kyeongnam 660-701, Republic of Korea

Received 5 March 2003; received in revised form 22 July 2003; accepted 2 October 2003

Abstract

On the basis of Eu's generalized hydrodynamics, a computational model is developed for the numerical simulation of rarefied and microscale diatomic gas flows. The rotational nonequilibrium effect is taken into account by introducing excess normal stress associated with the bulk viscosity of the gas. The computational model for diatomic gases reduces to the model for monatomic gases in the limit of vanishing bulk viscosity. The thermodynamically consistent computational model is applied to the one-dimensional shock wave structure and the two-dimensional hypersonic rarefied flow around a blunt body in order to demonstrate its capability and validate the numerical results. The general properties of the constitutive equations are also presented through a simple analysis. The numerical results show that the new generalized hydrodynamic computational model yields the solutions in qualitative agreement with experimental data and DSMC results in the case of the problems studied.

AMS: 65M06; 76N15; 76K05

Keywords: Rarefied and microscale gas dynamics; Diatomic gases; Generalized hydrodynamic equations; Finite volume method

1. Introduction

The study of nonlinear gas transport in rarefied condition [23,39] and microscale flows associated with MEMS [19] has emerged as an interesting topic of significance in recent years. It has been largely motivated by the need for a theoretical tool to efficiently predict aerothermodynamic loads on vehicles operating in high altitude and by the growing interest in the development of theory for microscale devices in MEMS. In the case of MEMS, the initial emphasis on the development of efficient fabrication techniques for microscale devices is now shifting towards the understanding of fundamental physical phenomena in such devices, which is critical in predicting their performance and in providing information on the optimal space

* Tel.: +82-55-751-6107; fax: +82-55-757-5622.
E-mail address: myong@nongae.gsnu.ac.kr (R.S. Myong).

0021-9991/$ - see front matter © 2003 Elsevier Inc. All rights reserved.
doi:10.1016/j.jcp.2003.10.015

within the huge design space. Thus the development of theoretical and computational models to predict the rarefied and microscale gas flows over the large portion of flow regimes is much desirable.

The primary physical parameter that characterizes the rarefied and microscale gas flows is the Knudsen number, and its value is not small in the aforementioned nonequilibrium flows, which occur in conditions far removed from equilibrium. Since the Navier–Stokes theory is capable of treating phenomena in a small deviation from local equilibrium and hence is not known to remain valid in the flow regimes of large Knudsen number, much effort has been put into the development of computational models beyond the theory of linear constitutive relations, typically, representative of the Navier–Stokes theory of the classical hydrodynamics. The models, which have been employed for the aforementioned purpose, can be classified into two categories; the full kinetic model and fluid dynamics model. One of the most successful methods in the former category is the direct simulation Monte Carlo (DSMC) [6], and it has been extensively used for the computation of hypersonic rarefied gas flows. The computational cost is, however, very high in comparison with the fluid dynamic models, in particular, in regimes near continuum limit. Moreover, it is more akin to experiment than theory, being in the class of computer simulations. On the other hand, the fluid dynamics models are based on the hyperbolic conservation laws and nonconserved variables appearing in the conservation laws, the latter being determined by their evolution equations which can be derived with the help of the Boltzmann equation.

By far several models have been developed for the latter category. This category may be subdivided into a few classes: in one of them the Burnett-type equations [9,30,39] are used for devising computational models; in another Grad's moment equations [20,25] are employed in conjunction with extended thermodynamics; and in still another the moment equations serving the basis of the generalization of thermodynamics [1,2,15–18] have been used in a manner consistent with the laws of thermodynamics at every order of approximation employed. These models originate from the kinetic theory of gases and come under the general category of either the moment method of Maxwell [24] and Grad [20] or the Chapman–Enskog method [11]. These macroscopic models were developed from the Boltzmann equation for a dilute gas with emphasis put on the efficiency of the computational cost. However, in these models there are the question of whether the solutions are uniquely determined, whether it satisfies the basic physical laws such as the second law of thermodynamics, and whether proper boundary conditions can be developed, and to what degree of nonequilibrium it is valid. Whereas all these questions apply to the classes of the models based on Burnett-type equations and also to the class of the Grad moment equations used in the extended thermodynamics in the case of which the question of thermodynamic consistency does not apply, the last class requires examination of the boundary conditions and to what extent it can remain useful when the system is removed far from equilibrium.

Toward the aim of answering the aforementioned questions and, at the same time, developing an efficient multi-dimensional computational model which satisfies the second law of thermodynamics at every order of approximation it was found that Eu's generalized hydrodynamic theory [15,16] was judged to be best suited and hence was utilized in a previous work [27] on gas flow phenomena. It was shown that the model, which was developed for a monatomic gas, yields solutions for all Knudsen numbers and under any flow condition. The main emphasis was placed on the development of an efficient multi-dimensional numerical schemes for the highly nonlinear generalized hydrodynamic equations.

In this work, the aforementioned generalized hydrodynamic computational model for monatomic gases is extended to diatomic gases. Recently the generalized hydrodynamic equations for monatomic gases have been extended to include rigid diatomic gases in the study of ultrasonic wave absorption [17] and shock waves [2] in diatomic gases. These studies have been based on one-dimensional ordinary differential equations. For more general applications of the generalized hydrodynamic theories it is essential to have multi-dimensional models. We examine a multi-dimensional model within the framework of the generalized hydrodynamic equations in this work. The approach taken here is therefore similar to the one taken in the previous work [27]; namely, we take Eu's generalized hydrodynamic theory [18] for diatomic

fluids. The main difference between the previous and present work is the appearance of extra equations in the set of evolution equations of nonconserved variables, which are related to the bulk viscosity, and the ultimate origin of the extra equations can be traced to the internal degrees of freedom related to the rotational motion of diatomic gas molecules. In the temperature regime where the rotational relaxation is much faster than hydrodynamic relaxations the rotational nonequilibrium effect can be simply taken into account by introducing excess normal stress associated with the bulk viscosity of the gas [13,17]. The explicit mechanism of rotational energy relaxation therefore is not included in the present work on the ground that the rotational energy relaxes at a much shorter time scale than the hydrodynamic relaxation time scale [17]. In addition, since the primary concern in the present work is to develop a computational method for describing the translational and rotational nonequilibrium effects in diatomic gases, the high temperature gas effects such as vibrational excitation and dissociation are omitted in the formulation for the sake of simplicity. However, the vibrational nonequilibrium effect will play a non-negligible role in the temperature range whose maximum is much higher than the onset temperature for vibrational excitation (800–1000 K) [4]. For the shock structure problem, depending on the upstream temperature, the critical Mach number of vibrational excitation can be in the range of 6 (125 K)–10 (50 K). For this reason, the detailed comparison with the experimental data will be concentrated on the range below this critical Mach number. A simple slip model, which is essential in the efficient computational simulation of a problem of technical interests, is also introduced for the diatomic gas and surface molecule interaction. The new computational model for diatomic gases readily reduces to the model for monatomic gases in the limit of vanishing bulk viscosity. Therefore the new model for diatomic gas flows shares the basis of the computational algorithm with the model for monatomic gas flows. This feature will make it possible to develop the new computational code from the code for monatomic gas in a very efficient way. The present new code, in fact, is inclusive of the computational model for monatomic gases reported in this journal previously [27].

The present paper is organized as follows. First, the main characteristics of Eu's generalized hydrodynamic theory are summarized in the hope that they can help the reader see the essential idea behind the theory, which appears at first glance very complicated and consequently its importance has not been fully recognized in the fluid dynamics community. The present summary will follow the kinetic derivation of the generalized hydrodynamic equations because it gives more insight when it is compared with other theories. For the description of the purely phenomenological derivation and the detailed discussion of Eu's generalized hydrodynamic theory, the reader is referred to his original work [1,2,15–18]. Then a generalized hydrodynamic computational model for diatomic gases and slip boundary conditions are introduced. In Section 3 computational algorithms for the model and the solutions of constitutive equations are described in detail. In Section 4 numerical results for the shock wave structure and the two-dimensional hypersonic rarefied gas flow around a blunt body are presented to demonstrate the capability of the generalized hydrodynamics model and to validate the numerical results thereof. Finally concluding remarks are given in Section 5.

2. A generalized hydrodynamic computational model for diatomic gases

2.1. Eu's generalized hydrodynamic equations

The Boltzmann–Curtiss kinetic equation for the diatomic molecule with a moment of inertia I and an angular momentum $\mathbf{j}$ can be expressed, under the assumption of no external field, as [12,17]

$$\left(\frac{\partial}{\partial t}+\mathbf{v}\cdot\nabla+\frac{j}{I}\frac{\partial}{\partial\psi}\right)f(\mathbf{v},\mathbf{r},\mathbf{j},\psi,t)=R[f]. \tag{1}$$

In this equation f, $\mathbf{v}$, $\mathbf{r}$, ψ, j, and $R[f]$ represent the distribution function, the particle velocity, the position, the azimuthal angle associated with the orientation of the molecule, the magnitude of the angular momentum vector $\mathbf{j}$, the collision integral, respectively. In addition to conservation laws of mass, momentum, and energy, the evolution equation for nonconserved variables can be derived by defining the following velocity moments and then calculating their time derivatives with the help of the Boltzmann–Curtiss kinetic equation. Define the moments by the statistical mechanical formula

$$\Phi^{(k)} = \langle h^{(k)} f \rangle, \tag{2}$$

where the angular brackets stand for integration over the variables $\mathbf{v}$ and j and $h^{(k)}$ denote the molecular expressions for moments whose form will be specified later in this section. Differentiating it with time and employing the Boltzmann–Curtiss equation we obtain the evolution equation for the kth nonconserved macroscopic variables $\Phi^{(k)}$

$$\rho \frac{\mathrm{D}(\Phi^{(k)}/\rho)}{\mathrm{D}t} + \nabla \cdot \psi^{(k)} = Z_k + \Lambda_k, \tag{3}$$

where $\psi^{(k)}$, the flux of $\Phi^{(k)}$, represents higher-order moments defined by

$$\psi^{(k)} = \langle \mathbf{C} h^{(k)} f \rangle \tag{4}$$

with $\mathbf{C}$ denoting the peculiar velocity of the molecule defined by $\mathbf{C} = \mathbf{v} - \mathbf{u}$, relative to the average bulk velocity $\mathbf{u}$; Z_k is the kinematic term arising from the hydrodynamic streaming effect; and Λ_k is the dissipation term which accounts for the energy dissipation accompanying the irreversible process. The ρ and $\mathrm{D}/\mathrm{D}t$ represent the density and the substantial time derivative, respectively. The only term in the evolution equation which is directly related to the details of the collision term in the kinetic equation is the dissipation term Λ_k, and it is defined in terms of the collision term $R[f]$ of the kinetic equation by the formula

$$\Lambda_k = \langle h^{(k)} R[f] \rangle. \tag{5}$$

This is the seat of energy dissipation that arises from the irreversible processes in the system, and at the molecular level the energy dissipation occurs in the system through molecular collisions. Therefore it is important to treat this term carefully before any assumption or approximation is made if we are to comprehend properly the energy dissipation mechanism of the system in a manner consistent with the principles of thermodynamics. Eu [15,16] developed the formal mathematical structure of nonequilibrium entropy (i.e., calortropy [16]) and irreversible thermodynamics consistent with the second law of thermodynamics by employing the nonequilibrium canonical distribution function

$$f^{\mathrm{c}} = \exp\left[-\frac{1}{k_{\mathrm{B}} T} \left(\frac{1}{2} m C^2 + H_{\mathrm{rot}} + \sum_{k=1}^{\infty} X_k h^{(k)} - \mu \right) \right]. \tag{6}$$

In this expression μ is the normalization factor; X_k are the conjugate variables to $h^{(k)}$ (their role is similar to the coefficients of the conventional moment expansion method); T is the temperature; k_{B} is the Boltzmann constant; m is the molecular mass; and H_{rot} denotes the rotational Hamiltonian of the molecule. The advantage of this exponential form of the distribution function is obvious; in the physical sense it is the only form that satisfies the additive property of the entropy and entropy production as well as the calortropy and calortropy production, all of which are in the logarithmic form of distribution function; in the mathematical sense it assures the non-negativity of the distribution function regardless of the level of approximations. By inserting the canonical form (6) into the definition of the dissipation term (5) and introducing the so-called cumulant expansion method [15,16], it can be shown that the dissipative term becomes the

form of a hyperbolic sine function $q(\kappa)$ of the Rayleigh dissipation function κ whose form will be presented at the end of this section.

The evolution equation (3) is an open system of partial differential equations, so that a closure must be introduced before any attempt of using it as a mathematical tool for the description of nonequilibrium hydrodynamic gas transport is made. There exist various methods to achieve this goal, for example, Grad's closure, but it is generally accepted that there exists no single closure theory founded on a firm theoretical justification and the effectiveness of the model highly depends on the details of the dissipative term.

The present work, for mathematical simplicity, will follow closely the Eu's approach, which remains within the framework of the first 13 moments, but takes a closure different from Grad's. The basic tenet taken for the closure used in Eu's approach is that since higher order moments decay faster than the conserved moments there is only a small number of moments necessary for the description of transport processes and the moments excluded from the subspace of macroscopic variables chosen for the description of the process of interest should not be calculated in terms of the moments belonging in the subspace chosen. The generalized hydrodynamic model presented has been devised according to this tenet. It is possible that other more complicated closures may be introduced, but it will be only at the cost of computational efficiency. The first assumption made in this work is that in the conditions examined experimentally – rarefied and microscale gas transport, for example, shock waves – the internal degrees of freedom relax much faster than the hydrodynamic modes. This implies that the evolution equation of the rotational energy may be suppressed in the present theory. Instead of explicitly taking into account the rotational relaxation mechanism, its effect is described with the help of the bulk viscosity which is directly related to the rotational degrees of freedom. However, for the problem that some physical parameters, such as the frequency of an external force in sound wave absorption and dispersion are comparable to the hydrodynamic scales, the evolution equations of rotational modes should be retained. Inclusion of such equations in the model is fairly straightforward.

By the first assumption the infinite set of nonconserved moments in the evolution equation can be truncated to the following set,

$$\Phi^{(1)} = \mathbf{\Pi}, \quad \Phi^{(2)} = \Delta, \quad \Phi^{(3)} = \mathbf{Q},$$

$$h^{(1)} = m[\mathbf{CC}]^{(2)}, \quad h^{(2)} = \frac{1}{3}mC^2 - p/n, \quad h^{(3)} = \left[\frac{1}{2}mC^2 + H_{\mathrm{rot}} - m\hat{h}\right]\mathbf{C}.$$

In this expression, $\mathbf{\Pi}$, Δ, $\mathbf{Q}$ represent the shear stress, the excess normal stress, the heat flux, and the stresses are related to the stress tensor $\mathbf{P}$ through the relation

$$\mathbf{P} = (p + \Delta)\mathbf{I} + \mathbf{\Pi}, \tag{7}$$

where $\mathbf{I}$ denotes the unit second-rank tensor. The equation of state $p = nk_{\mathrm{B}}T$ is also assumed, where p and n are the pressure and the number density of the molecules. The $\hat{h}$ represents the enthalpy density per unit mass and the symbol $[\mathbf{A}]^{(2)}$ denotes the traceless symmetric part of the second-rank tensor $\mathbf{A}$,

$$[\mathbf{A}]^{(2)} = \frac{1}{2}(\mathbf{A} + \mathbf{A}^{\mathrm{t}}) - \frac{1}{3}\mathbf{I}\mathrm{Tr}\mathbf{A}. \tag{8}$$

The second assumption made in this work is that the relaxation times of the nonconserved variables $(\mathbf{\Pi}, \Delta, \mathbf{Q})$ are very short in comparison with the conserved variables such as the density and velocity. In other words, the stress evolves much faster than the velocity does. As a matter of fact, this assumption is based on the kinetic theory computation of the relaxation times in the absence of an oscillating external field. Owing to the short time scale of evolution, if the system is allowed to evolve from a nonequilibrium state characterized by non-vanishing nonconserved variables, the latter will have already reached their

steady state on the hydrodynamic time scale, resulting in $\mathrm{D}(\Phi^{(k)}/\rho)/\mathrm{D}t = 0$, while the conserved variables are still slowly evolving. Together with this so-called adiabatic approximation the application of the Eu closure yields the following closure relation in Eu's formulation of generalized hydrodynamics in which the nonconserved variables are at the steady state,

$$\rho \frac{\mathrm{D}(\Phi^{(k)}/\rho)}{\mathrm{D}t} + \nabla \cdot \psi^{(k)} = 0. \tag{9}$$

Then it can be shown that, after applying a simplification to the convective term in the evolution equation of the heat flux which is consistent with the adiabatic approximation, the evolution equation (3) reduces to the forms [18]

$$-2(p+\Delta)[\nabla \mathbf{u}]^{(2)} - 2[\boldsymbol{\Pi} \cdot \nabla \mathbf{u}]^{(2)} - \frac{p}{\eta}\boldsymbol{\Pi} q(\kappa) = 0, \tag{10}$$

$$-2\gamma'(\Delta \mathbf{I} + \boldsymbol{\Pi}) : \nabla \mathbf{u} - \frac{2}{3}\gamma' p \nabla \cdot \mathbf{u} - \frac{2}{3}\gamma' \frac{p}{\eta_\mathrm{b}} \Delta q(\kappa) = 0, \tag{11}$$

$$-(p+\Delta) C_\mathrm{p} T \nabla \ln T - \boldsymbol{\Pi} \cdot C_\mathrm{p} \nabla T - \mathbf{Q} \cdot \nabla \mathbf{u} - \frac{p C_\mathrm{p} T}{\lambda} \mathbf{Q} q(\kappa) = 0, \tag{12}$$

where

$$q(\kappa) = \frac{\sinh \kappa}{\kappa}$$

with the dissipation function κ given by the formula

$$\kappa = \frac{(m k_\mathrm{B})^{1/4}}{\sqrt{2} d} \frac{T^{1/4}}{p} \left[\frac{\boldsymbol{\Pi} : \boldsymbol{\Pi}}{2\eta} + \gamma' \frac{\Delta^2}{\eta_\mathrm{b}} + \frac{\mathbf{Q} \cdot \mathbf{Q}}{\lambda} \right]^{1/2}.$$

Here $\gamma' = (5 - 3\gamma)/2$, where γ is the specific heat ratio and d and C_p denote the diameter of the molecule and the heat capacity per mass at constant pressure, respectively. The term $[\boldsymbol{\Pi} \cdot \nabla \mathbf{u}]^{(2)}$ represents the coupling between the shear stress and velocity gradient and its components can be derived by using the definition of operation $[]^{(2)}$ in Eq. (8). The η, η_b and λ are the Chapman–Enskog shear viscosity, bulk viscosity, and thermal conductivity, respectively, of the diatomic molecule. The dissipation function κ is the first-order cumulant of the cumulant approximation for dissipation terms [15,16]. The colon in κ denotes the double scalar product between tensors, namely, contraction to a scalar.

Together with the aforementioned evolution equations the following conservation laws can be applied to various applications as the governing equations for nonequilibrium diatomic gas flows,

$$\begin{pmatrix} \rho \\ \rho \mathbf{u} \\ \rho E \end{pmatrix}_\mathrm{t} + \nabla \cdot \begin{pmatrix} \rho \mathbf{u} \\ \rho \mathbf{u}\mathbf{u} + p\mathbf{I} \\ (\rho E + p)\mathbf{u} \end{pmatrix} + \nabla \cdot \begin{pmatrix} 0 \\ \boldsymbol{\Pi} + \Delta \mathbf{I} \\ (\boldsymbol{\Pi} + \Delta \mathbf{I}) \cdot \mathbf{u} + \mathbf{Q} \end{pmatrix} = 0, \tag{13}$$

where E represents the total energy density.

2.2. A generalized hydrodynamic computational model

On the basis of the adiabatic approximation of Eu's generalized hydrodynamic equations (10)–(12) presented in the previous section, a generalized hydrodynamic computational model for diatomic gases can be developed. If the following dimensionless variables and parameters are used

$$t^* = t/(L/u_r), \quad \mathbf{x}^* = \mathbf{x}/L, \quad \eta^* = \eta/\eta_r, \quad \lambda^* = \lambda/\lambda_r, \quad \mathbf{u}^* = \mathbf{u}/u_r,$$

$$\rho^* = \rho/\rho_r, \quad T^* = T/T_r, \quad p^* = p/p_r, \quad E^* = E/u_r^2,$$

$$\mathbf{\Pi}^* = \mathbf{\Pi}/(\eta_r u_r/L), \quad \Delta^* = \Delta/(\eta_{b_r} u_r/L), \quad \mathbf{Q}^* = \mathbf{Q}/(\lambda_r \Delta T/LT_r)$$

the dimensionless evolution equations of a diatomic gas in the generalized hydrodynamics can be written as

$$\frac{\partial \mathbf{U}}{\partial t} + \nabla \cdot \mathbf{F}_T = 0 \tag{14}$$

and

$$\hat{\mathbf{\Pi}} q(c\hat{R}) = (1 + f_b \hat{\Delta})\hat{\mathbf{\Pi}}_0 + [\hat{\mathbf{\Pi}} \cdot \nabla \hat{\mathbf{u}}]^{(2)}, \tag{15}$$

$$\hat{\Delta} q(c\hat{R}) = \hat{\Delta}_0 + \frac{3}{2} f_b (\hat{\mathbf{\Pi}} + f_b \hat{\Delta}\mathbf{I}) : \nabla \hat{\mathbf{u}}, \tag{16}$$

$$\hat{\mathbf{Q}} q(c\hat{R}) = (1 + f_b \hat{\Delta})\hat{\mathbf{Q}}_0 + \hat{\mathbf{\Pi}} \cdot \hat{\mathbf{Q}}_0. \tag{17}$$

Here $\hat{\mathbf{\Pi}}_0$, $\hat{\Delta}_0$ and $\hat{\mathbf{Q}}_0$ are determined by the Newtonian law of shear and bulk viscosity and the Fourier law of heat conduction, respectively,

$$\mathbf{\Pi}_0 = -2\eta[\nabla \mathbf{u}]^{(2)}, \quad \Delta_0 = -\eta_b \nabla \cdot \mathbf{u}, \quad \mathbf{Q}_0 = -\lambda \nabla \ln T. \tag{18}$$

It should be noted that the so-called second coefficient of viscosity in the Stokes' hypothesis [36] is equivalent to

$$\eta_b - \frac{2}{3}\eta.$$

The asterisks are omitted from the aforementioned equations for notational brevity. The matrices and other variables are defined as

$$\mathbf{U} = \begin{pmatrix} \rho \\ \rho \mathbf{u} \\ \rho E \end{pmatrix},$$

$$\mathbf{F} = \begin{pmatrix} \rho \mathbf{u} \\ \rho \mathbf{u}\mathbf{u} + \frac{1}{\gamma M^2} p \mathbf{I} \\ (\rho E + \frac{1}{\gamma M^2} p)\mathbf{u} \end{pmatrix}, \quad \mathbf{F}_v = \frac{1}{Re} \begin{pmatrix} 0 \\ \mathbf{\Pi} + f_b \Delta \mathbf{I} \\ (\mathbf{\Pi} + f_b \Delta \mathbf{I}) \cdot \mathbf{u} + \frac{1}{Ec\,Pr} \mathbf{Q} \end{pmatrix},$$

$$\hat{\mathbf{\Pi}} \equiv \frac{N_\delta}{p} \mathbf{\Pi}, \quad \hat{\Delta} \equiv \frac{N_\delta}{p} \Delta, \quad \hat{\mathbf{Q}} \equiv \frac{N_\delta}{p} \frac{\mathbf{Q}}{\sqrt{T/(2\epsilon)}},$$

$$\nabla \hat{\mathbf{u}} \equiv -2\eta \frac{N_\delta}{p} \nabla \mathbf{u}, \quad \epsilon \equiv \frac{1}{Pr\,Ec\,T_r/\Delta T},$$

and $q(c\hat{R})$ is a nonlinear factor defined by

$$q(c\hat{R}) = \frac{\sinh(c\hat{R})}{c\hat{R}},$$

$$\hat{R}^2 \equiv \hat{\mathbf{\Pi}} : \hat{\mathbf{\Pi}} + \frac{2\gamma'}{f_b}\hat{\Delta}^2 + \hat{\mathbf{Q}} \cdot \hat{\mathbf{Q}}.$$

The $\mathbf{U}$ is the vector made up of conserved variables and $\mathbf{F}_T$ represents the sum of the inviscid flux vector $\mathbf{F}$ and the viscous flux vector $\mathbf{F}_v$. It should be mentioned that in the present work the term $\mathbf{Q} \cdot \nabla \mathbf{u}$ appearing in the constitutive relation of heat flux (12) is omitted in the computational model (17) for the sake of simplicity. The M, Re, Ec, and Pr are dimensionless fluid dynamic numbers; Mach, Reynolds, Eckert, and Prandtl number, respectively. f_b represents the ratio of the bulk viscosity to the shear viscosity. Its value can be determined by the sound wave absorption measurement. The value for nitrogen is 0.8 according to the experiment [17]. The caret ^ over a symbol represents a quantity with the dimension of the ratio of the stress to the pressure. The subscript r stands for the reference state; for example, the state of the inflow condition. The constant c, which is given by

$$c = \left[\frac{2\sqrt{\pi}}{5} A_2(v) \Gamma[4 - 2/(v-1)]\right]^{1/2} \tag{19}$$

has a value between 1.0138 (Maxwellian) and 1.2232 ($v = 3$), where v is the exponent of the inverse power law for the gas particle interaction potential and Γ denotes the gamma function. The η, η_b and λ can be expressed as $\eta = T^s$, $\eta_b = f_b\eta$, $\lambda = T^{s+1}$ where $s = \frac{1}{2} + 2/(v-1)$.

For a perfect gas the following dimensionless relations hold,

$$p = \rho T, \quad \rho E = \frac{p/\gamma \mathrm{M}^2}{\gamma - 1} + \frac{1}{2}\rho \mathbf{u} \cdot \mathbf{u}. \tag{20}$$

A composite number, which is defined by [15,16,18]

$$N_\delta \equiv \frac{\eta_r u_r / L}{p_r} = \gamma \frac{M^2}{Re} = KnM\sqrt{\frac{2\gamma}{\pi}}$$

measures the magnitude of the viscous stress relative to the hydrostatic pressure, so that it indicates the degree of departure from equilibrium. As N_δ becomes small, the Newtonian law of viscosity and the Fourier law of heat conduction are recovered [15,16,18] from the constitutive relations (15)–(17):

$$\mathbf{\Pi} = \mathbf{\Pi}_0, \quad \Delta = \Delta_0, \quad \mathbf{Q} = \mathbf{Q}_0.$$

If the Stokes hypothesis – which is nothing but neglecting the bulk viscosity – is applied, the aforementioned laws of viscosity and heat conduction yield the well-known Navier–Stokes constitutive equations:

$$\mathbf{\Pi} = \mathbf{\Pi}_0, \quad \mathbf{Q} = \mathbf{Q}_0.$$

It will be shown, however, in latter section that this common practice in aerodynamic theories can significantly affect the results for some phenomena and, in particular, for the shock wave structure, as will be shown later.

For a diatomic gas, $\gamma = \frac{7}{5}$ and $Pr = \frac{14}{19}$ through Eucken's relation

$$Pr = \frac{4\gamma}{9\gamma - 5}.$$

2.3. Boundary conditions

For slip models for the gas–surface molecular interaction, the so-called Langmuir slip model has been employed in the previous works [5,14,27]. They can be expressed, in the dimensional form, as

$$u = \alpha u_{\mathrm{w}} + (1-\alpha)u_{\mathrm{g}}, \tag{21}$$

$$T = \alpha T_{\mathrm{w}} + (1-\alpha)T_{\mathrm{g}}, \tag{22}$$

where

$$\alpha = \frac{\beta p}{1+\beta p}. \tag{23}$$

The subscript w stands for the wall and the subscript g denotes the local value adjacent to the wall – a mean free path away from the wall. The parameter β depends on the wall temperature T_{w} and the interfacial interaction parameters. By imagining the gas–surface molecule interaction process as a chemical reaction, it is possible to express the parameter β in the form

$$\beta = \frac{A l_{\mathrm{r}}}{k_{\mathrm{B}} T_{\mathrm{w}}} \exp\left(\frac{D_{\mathrm{e}}}{k_{\mathrm{B}} T_{\mathrm{w}}}\right) \cdot \frac{\ell}{l_{\mathrm{r}}}, \tag{24}$$

where A is the mean area of a site, and D_{e} is the potential parameter. These parameters can be inferred from experimental data or theoretical consideration of intermolecular forces and the surface–molecule interaction. l is the mean free path and ℓ is a mean collision distance between the wall surface and the gas molecules at all angles. When the characteristic length L is taken equal to ℓ, the ℓ/l_{r} becomes $1/Kn$. This parameter can be simplified into, after some manipulation,

$$\beta = \sqrt{\frac{\pi}{32}} \frac{A}{c^2 d_{\mathrm{STP}}^2} \left[\frac{T_{\mathrm{r}}}{273}\right]^{(2/(\nu-1))} \frac{T_{\mathrm{r}}}{T_{\mathrm{w}}} \exp\left(\frac{D_{\mathrm{e}}}{k_{\mathrm{B}} T_{\mathrm{w}}}\right) \frac{1}{p_{\mathrm{r}} Kn}. \tag{25}$$

If A is approximated as $\pi d^2/4$, the parameter β becomes

$$\beta = \sqrt{\frac{\pi}{32}} \frac{\pi}{c^2} \frac{T_{\mathrm{r}}}{T_{\mathrm{w}}} \exp\left(\frac{D_{\mathrm{e}}}{k_{\mathrm{B}} T_{\mathrm{w}}}\right) \frac{1}{p_{\mathrm{r}} Kn}. \tag{26}$$

This model can be easily extended to the case of the adsorption of a diatomic gas such as nitrogen on a metallic surface [28]. If we assume multimolecular (double) layer on solid surfaces, the resulting relation of α simply becomes

$$\alpha = \frac{\sqrt{\beta p}}{1+\sqrt{\beta p}}. \tag{27}$$

For an Ar–Al molecular interaction model and a N_2–Al molecular interaction model, the following data may be used:

$$D_{\mathrm{e}} = 1.32 \text{ kcal/mol}.$$

3. Computational algorithms

3.1. Finite volume formulation

The generalized hydrodynamic equations (14)–(17) satisfy the following collision-free hyperbolic conservation laws,

$$\frac{\partial}{\partial t}\int_V \mathbf{U}\,\mathrm{d}V + \oint_S \mathbf{F}_\mathrm{T}\cdot\mathbf{n}\,\mathrm{d}S = 0,$$

where S represents the bounding surface of the control volume V. Most of modern CFD schemes based on the hyperbolic conservation laws can be applied to treating these equations. In the present study, the upwind scheme with van Leer's flux vector splitting solver [31] is used. The one-dimensional discretized form of the hyperbolic conservation laws in the finite volume formulation can be expressed as

$$\mathbf{U}_i^{n+1} = \mathbf{U}_i^n - \frac{\Delta t}{\Delta x}\left[\mathbf{F}^n_{T_{i+\frac{1}{2}}} - \mathbf{F}^n_{T_{i-\frac{1}{2}}}\right], \tag{28}$$

where $\mathbf{U}$ is the cell-averaged conserved variables, Δx is the size of i-cell, Δt is the time step, and $\mathbf{F}_\mathrm{T}$ is the numerical flux function which gives the flux through cell interfaces. Second-order accuracy can be obtained by using the MUSCL-Hancock method [32].

The numerical flux through the interface in the discretized equation in general non-Cartesian domains can be determined by exploiting the rotational invariance of the conservation laws (14). Let us consider the kth intercell boundary ΔL_k of finite area $A_{i,j}$ in two-dimensional (x,y) space. Let $(\mathbf{n},\mathbf{s})_k$ be the outward unit vector normal to the kth boundary, and the unit vector tangent to the kth boundary with the convention that the interior of the volume always lies on the left hand side of the boundary. If θ_k is defined as the angle formed by the x-direction and the normal vector $\mathbf{n}_k$ it can be shown that the discretized equation becomes

$$\mathbf{U}_{i,j}^{n+1} = \mathbf{U}_{i,j}^n - \frac{\Delta t}{A_{i,j}}\sum_{k=1}^{N}\mathbf{R}_k^{-1}\mathbf{F}^n_{T_k}\Delta L_k, \tag{29}$$

where

$$\mathbf{U}_{i,j} = \begin{pmatrix}\rho\\ \rho u\\ \rho v\\ \rho E\end{pmatrix}_{i,j}, \quad \mathbf{F}_k = \begin{pmatrix}\rho u_n\\ \rho u_n^2 + \frac{1}{\gamma M^2}p\\ \rho u_n u_s\\ (\rho E + \frac{1}{\gamma M^2}p)u_n\end{pmatrix}_k,$$

$$\mathbf{F}_{v_k} = \frac{1}{Re}\begin{pmatrix}0\\ \Pi_{nn} + f_\mathrm{b}\Delta\\ \Pi_{ns}\\ (\Pi_{nn} + f_\mathrm{b}\Delta)u_n + \Pi_{ns}u_s + \frac{1}{Ec\,Pr}Q_n\end{pmatrix}_k,$$

and $\mathbf{R}_k \equiv \mathbf{R}(\theta_k)$ is the rotation matrix, namely,

$$\mathbf{R}(\theta) = \begin{pmatrix}1 & 0 & 0 & 0\\ 0 & \cos\theta & \sin\theta & 0\\ 0 & -\sin\theta & \cos\theta & 0\\ 0 & 0 & 0 & 1\end{pmatrix}.$$

The N is the number of interfaces in a cell. In this process a transformation law between the components of the tensor in the (x, y) coordinates ($\mathbf{\Pi}$) and the components of the tensor in the (n, s) coordinates ($\tilde{\mathbf{\Pi}}$) is used.

$$\mathbf{\Pi} = \mathbf{R}^{-1}\tilde{\mathbf{\Pi}}\mathbf{R}. \tag{30}$$

3.2. Computations of constitutive equations

In order to solve the discretized equation (29) of the conservation laws (14) an algorithm to solve the nonlinear algebraic system of constitutive relations (15)–(17) is necessary. It provides the stress and heat flux, which are essential to define the numerical flux through cell interfaces. This process becomes trivial in the Navier–Stokes equations since the stress and heat flux are proportional to the thermodynamic forces. However, owing to the nonlinearity of the constitutive equations an additional process must be developed in the present method. Here an iterative method will be developed to solve the constitutive equations for given thermodynamic variables (pressure and temperature) and the gradients of velocity and temperature. This is in sharp contrast with other moment methods, for example, the extended thermodynamics of Müller et al. [25] in which the constitutive equations are derived in a way that the whole system is of hyperbolic type. In fact, the present numerical method shares more common features with the Navier–Stokes method than other methods in the sense that the overall system is of parabolic type rather than of hyperbolic type. This makes it possible to develop a numerical code whose basic building blocks is the same as the Navier–Stokes code. An additional step is needed only when stress and heat flux appearing in the flux of the system are calculated from the nonlinear algebraic constitutive equations.

In general, the constitutive equations (15)–(17) consist of 10 equations of (Π_{xx}, Π_{xy}, Π_{xz}, Π_{yy}, Π_{yz}, Π_{zz}, Δ, Q_x, Q_y, Q_z) for known 14 parameters ($p, T, \nabla u$, ∇v, ∇w, ∇T). Owing to the highly nonlinear terms, it appears to be difficult to develop a proper numerical method for solving the equations. Nevertheless, it can be shown that they can be solved by a numerical method in the case of a one-dimensional problem.

In the case of a two-dimensional problem the stress and heat flux components (Π_{xx}, Π_{xy}, Δ, Q_x) on a line in the two-dimensional physical plane induced by thermodynamic forces (u_x, v_x, T_x) can be approximated as the sum of two solvers: (1) one on ($u_x, 0, T_x$), and (2) another on $(0, v_x, 0)$. It can be shown that the equations for the first solver, which describe the compression and expansion of a diatomic gas, are given by:

$$\hat{\Pi}_{xx}q(c\hat{R}) = (\hat{\Pi}_{xx} + f_b\hat{\Delta} + 1)\hat{\Pi}_{xx_0}, \tag{31}$$

$$\hat{\Delta}q(c\hat{R}) = [3(\hat{\Pi}_{xx} + f_b\hat{\Delta}) + 1]\hat{\Delta}_0, \tag{32}$$

$$\hat{Q}_x q(c\hat{R}) = (\hat{\Pi}_{xx} + f_b\hat{\Delta} + 1)\hat{Q}_{x_0}, \tag{33}$$

where

$$\hat{R}^2 = \frac{3}{2}\hat{\Pi}_{xx}^2 + \frac{4}{5f_b}\hat{\Delta}^2 + \hat{Q}_x^2,$$

$$\hat{\Delta}_0 = \frac{3}{4}f_b\hat{\Pi}_{xx_0}.$$

The following relation between the xx-component of the shear stress and the excess normal stress can be obtained by combining the first two equations

$$\hat{\Delta} = \frac{1}{8f_b}[(9f_b^2 - 4)\hat{\Pi}_{xx} - 4 + \sqrt{D}],$$

where

$$D = (81f_b^4 + 72f_b^2 + 16)\hat{\Pi}_{xx}^2 + (32 - 24f_b^2)\hat{\Pi}_{xx} + 16.$$

The following constitutive relations for the second solver, which describe the shear flow,

$$\hat{\Pi}_{xx}q(c\hat{R}) = -\frac{2}{3}\hat{\Pi}_{xy}\hat{\Pi}_{xy_0}, \tag{34}$$

$$\hat{\Pi}_{xy}q(c\hat{R}) = (1 + \hat{\Pi}_{xx} + f_b\hat{\Delta})\hat{\Pi}_{xy_0}, \tag{35}$$

$$\hat{\Delta}q(c\hat{R}) = 3f_b\hat{\Pi}_{xy}\hat{\Pi}_{xy_0} \tag{36}$$

yield an equation of one variable $\hat{\Pi}_{xx}$ and an additional equation for $\hat{\Delta}$

$$\hat{\Pi}_{xx}q^2(c\hat{R}) = -\frac{2}{3}\left[\left(1 - \frac{9}{2}f_b^2\right)\hat{\Pi}_{xx} + 1\right]\hat{\Pi}_{xy_0}^2, \tag{37}$$

$$\hat{\Delta} = -\frac{9}{2}f_b\hat{\Pi}_{xx}, \tag{38}$$

where

$$\hat{R}^2 = 3\hat{\Pi}_{xx}\left[\left(1 + \frac{45}{4}f_b^2\right)\hat{\Pi}_{xx} - 1\right],$$

which follows from the stress constraint

$$\hat{\Pi}_{xy} = \mathrm{sign}(\hat{\Pi}_{xy_0})\left[-\frac{3}{2}\left[\left(1 - \frac{9}{2}f_b^2\right)\hat{\Pi}_{xx} + 1\right]\hat{\Pi}_{xx}\right]^{1/2}. \tag{39}$$

It should be noted that the range of the bulk viscosity represented by f_b has no effect on the mathematical structure of the constitutive equations of the gas compression and expansion problem, but it has significant effects on that of the shear flow problem. It can be easily shown that the stress constraint of the shear flow problem changes its mathematical type from ellipse to hyperbola at the critical point

$$f_b = \frac{\sqrt{2}}{3}.$$

The constitutive equations (34)–(36) and (37)–(39) for a diatomic gas can be solved by extending the method of iteration [26,27], which is originally developed for a monatomic gas. All the calculations turned out to provide converged solutions within a few iterations. The iteration procedures can be summarized as follows. In the solver on $(u_x, 0, T_x)$, for positive $\hat{\Pi}_{xx_0}$ and $\hat{Q}_{x_0}$

$$\hat{R}_{n+1} = \frac{1}{c}\sinh^{-1}[c\sqrt{Y_n}],$$

where

$$Y_n \equiv (1 + \hat{\Pi}_{xx_n} + f_b\hat{\Delta}_n)^2\hat{R}_0^2 + 4(\hat{\Pi}_{xx_n} + f_b\hat{\Delta}_n)[1 + 2(\hat{\Pi}_{xx_n} + f_b\hat{\Delta}_n)]\frac{4}{5f_b}\hat{\Delta}_0^2$$

and

$$\hat{\Pi}_{xx_{n+1}} = \frac{(1 + \hat{\Pi}_{xx_n} + f_b\hat{\Delta}_n)\hat{\Pi}_{xx_0}}{\sqrt{Y_n}}\hat{R}_{n+1},$$

$$\hat{Q}_{x_{n+1}} = \frac{\hat{Q}_{x_0}}{\hat{\Pi}_{xx_0}}\hat{\Pi}_{xx_{n+1}},$$

and for negative $\hat{\Pi}_{xx_0}$ and $\hat{Q}_{x_0}$

$$\hat{\Pi}_{xx_{n+1}} = \frac{(1 + f_b\hat{\Delta}_n)\hat{\Pi}_{xx_0}}{q(c\hat{R}_n) - \hat{\Pi}_{xx_0}}$$

and

$$\hat{Q}_{x_{n+1}} = \frac{\hat{Q}_{x_0}}{\hat{\Pi}_{xx_0}}\hat{\Pi}_{xx_{n+1}}.$$

Since the equations are invariant under a transform $\hat{Q}_x \leftrightarrow -\hat{Q}_x$, only two cases satisfying $\hat{\Pi}_{xx}\hat{Q}_x > 0$ are considered. In these expressions $\hat{\Pi}_{xx_1}$, $\hat{\Delta}_1$, and $\hat{Q}_{x_1}$ are given by the equations

$$\hat{\Pi}_{xx_1} = \frac{\sinh^{-1}(c\hat{R}_0)}{c\hat{R}_0}\hat{\Pi}_{xx_0},$$

$$\hat{\Delta}_1 = \frac{\sinh^{-1}(c\hat{R}_0)}{c\hat{R}_0}\hat{\Delta}_0,$$

$$\hat{Q}_{x_1} = \frac{\sinh^{-1}(c\hat{R}_0)}{c\hat{R}_0}\hat{Q}_{x_0}.$$

In the second solver on $(0, v_x, 0)$ the $\hat{\Pi}_{xx}$ can be obtained for a given $\hat{\Pi}_{xy_0}$ through the equation

$$\hat{R}_{n+1} = \frac{1}{c}\sinh^{-1}[cY_n],$$

where

$$Y_n \equiv \left[2\left[1 + \left(1 - \frac{9}{2}f_b^2\right)\hat{\Pi}_{xx_n}\right]\left[1 - \left(1 + \frac{45}{4}f_b^2\right)\hat{\Pi}_{xx_n}\right]\right]^{1/2}\hat{\Pi}_{xy_0}$$

and

$$\hat{\Pi}_{xx_{n+1}} = \frac{2(3 - \sqrt{D_{n+1}})}{3(4 + 45f_b^2)}$$

where

$$D_{n+1} = 12\left(1 + \frac{45}{4}f_b^2\right)\hat{R}_{n+1}^2 + 9.$$

The term Y_n is well defined for any f_b greater than the critical value $\sqrt{2}/3$. The $\hat{\Delta}$ and $\hat{\Pi}_{xy}$ can be calculated by using Eq. (38) and the stress constraint (39).

When $0 \leqslant f_b < \sqrt{2}/3$, the process of calculating the $\hat{\Pi}_{xx}$ may be replaced by the following algorithm:

$$\hat{\Pi}_{xx_{n+1}} = -\frac{2\hat{\Pi}_{xy_0}^2}{3q^2(c\hat{R}_n) + (2 - 9f_b^2)\hat{\Pi}_{xy_0}^2},$$

where

$$\hat{R}_n = \left[3\hat{\Pi}_{xx_n}\left[\left(1 + \frac{45}{4}f_b^2\right)\hat{\Pi}_{xx_n} - 1\right]\right]^{1/2}.$$

The general properties of constitutive relations in the case of a diatomic gas are shown in Figs. 1–3. The generalized hydrodynamic constitutive relations in one-dimensional u_x-only problem are depicted in comparison with the Navier–Stokes theory in Fig. 1. Here, the heat flux is assumed to be equal to zero for the sake of simplicity. In contrast to the Navier–Stokes theory the asymmetry of the normal stress for rapid expansion and compression of gas is predicted by generalized hydrodynamics. Even though the details are slightly different, the general trend of the stresses for monoatomic and diatomic gases remains unchanged. The relationship between the shear stress and the excess normal stress in the u_x-only problem is shown in Fig. 2. The relationship is almost linear in the regime of compression of gas, while it becomes highly nonlinear in the regime of expansion of gas. Fig. 3 demonstrates that the shear stresses predicted by generalized hydrodynamics become very small compared to the Navier–Stokes theory as the tangential velocity gradient becomes very large. Such an asymptotic behavior indicates that the new constitutive relations have a correct free-molecular limit, implying that the velocity slip phenomenon caused by the

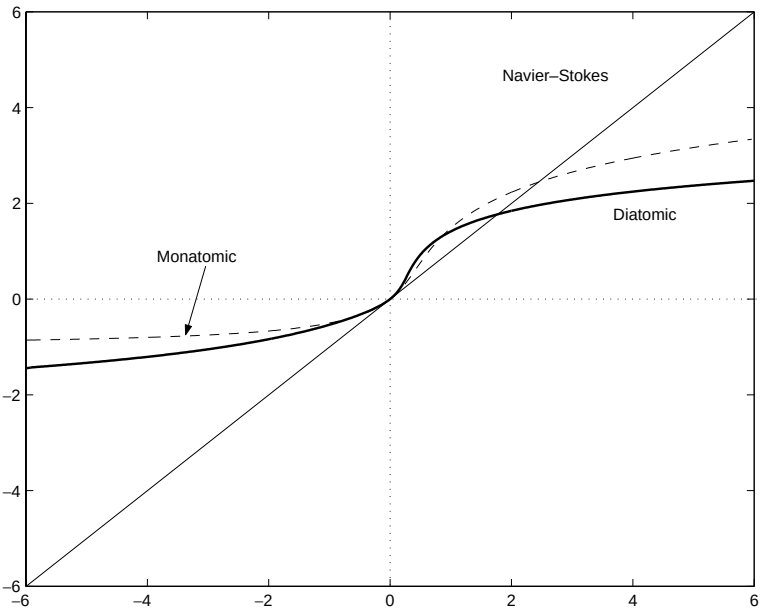

Fig. 1. Generalized hydrodynamic constitutive relations (diatomic and monatomic) relative to the Navier–Stokes relations in the u_x-only problem ($c = 1.0179$, $f_b = 0.8$, no heat flux). The horizontal and vertical axes represent the Navier–Stokes relations $\hat{\Pi}_{xx_0}$, and the relations $\hat{\Pi}_{xx}$, respectively. The gas is expanding in the range $\hat{\Pi}_{xx_0} < 0$, whereas the gas is compressed in the range of $\hat{\Pi}_{xx_0} > 0$.

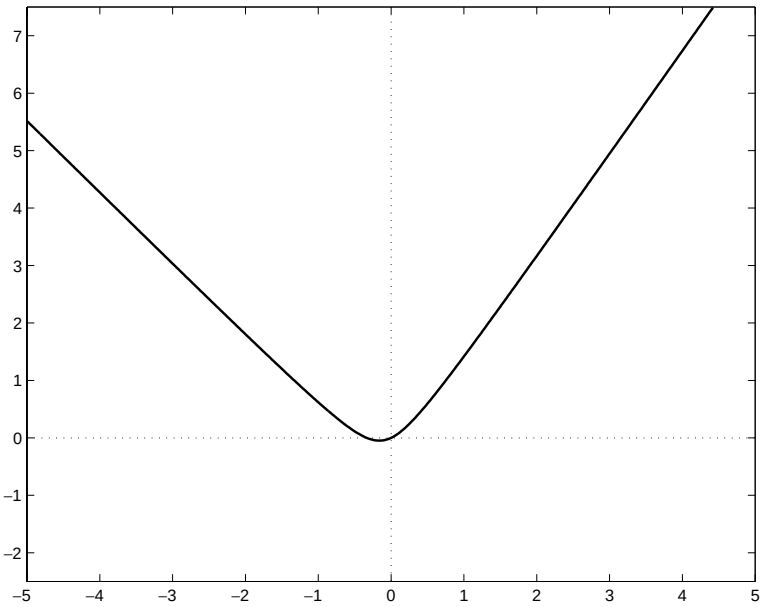

Fig. 2. The relationship between the shear stress $\hat{\Pi}_{xx}$ and the excess normal stress $\hat{\Delta}$ in the u_x-only problem. The horizontal and vertical axes represent $\hat{\Pi}_{xx}$, and the relations $\hat{\Delta}$, respectively.

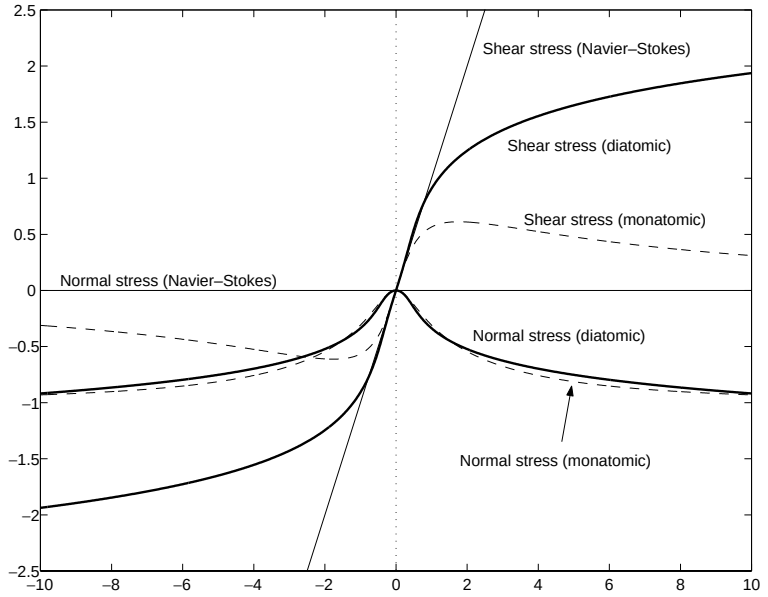

Fig. 3. Generalized hydrodynamic constitutive relations relative to the Navier–Stokes relations in the v_x-only problem ($c = 1.0179$, $f_b = 0.8$). The horizontal axis represents the velocity gradient $\hat{\Pi}_{xy_0}$. The vertical axis represents the normal ($\hat{\Pi}_{xx}$) and shear ($\hat{\Pi}_{xy}$) stresses.

non-Newtonian effect can be explained in a very simple way. The ultimate origin of this behavior can be traced to the kinematic term – specifically, the constraint equation (39) on the normal ($\hat{\Pi}_{xx}$) and shear ($\hat{\Pi}_{xy}$) stresses.

3.3. Numerical implementation

Since the steady-state solutions are obtained by the time-marching method, a proper stability condition is necessary. It turns out that for the present computational model the following condition for upwind schemes works well:

$$\Delta t = \mathrm{CFL} \cdot \min(\Delta t_1, \Delta t_2), \tag{40}$$

where

$$\Delta t_1 = \mathrm{M}\left[\frac{\Delta x}{|a|} + \frac{2\eta(1+0.8f_\mathrm{b})M}{\rho a^2}\right],$$

$$\Delta t_2 = \mathrm{M}\left[\frac{|a|}{\Delta x} + \frac{2\eta(1+0.8f_\mathrm{b})M}{\rho \Delta x^2}\right]^{-1}$$

and a denotes the speed of sound. For given T_w, T_r, u_w, u_r, and p_r, the boundary conditions and the mechanical balance condition (zero normal gradient of pressure) yield the boundary values of temperature, tangential velocity, and pressure. From these values the boundary value of the density can be determined by the perfect gas relation. The velocity normal to the surface can be assumed to be zero. For artificial boundaries, inflow and outflow conditions based on the number of Euler characteristics can be employed.

The discretized form of the generalized hydrodynamic equations in the finite volume formulation (29), a time step restriction (40), and the boundary conditions (21) and (22) are the basic building blocks of the present numerical method. It resembles numerical methods for the compressible Navier–Stokes equations in that they all share the hyperbolic conservation laws. The present scheme, however, differs from the latter methods in the manner of calculating the viscous flux. Since the stress and the heat flux are a nonlinear function of thermodynamic forces, they are determined with the help of the Eqs. (31)–(33) and (37)–(39).

4. Numerical experiment

The capability of the new model is tested by considering two problems: shock wave structure and two-dimensional hypersonic blunt body flow. The diatomic gas is assumed to be nitrogen ($s = 0.78$ in the coefficient of viscosity, $c = 1.0179$, $f_\mathrm{b} = 0.8$), which is virtually a rigid rotator in the temperature range of study. In general, the initial data necessary to define a well-posed problem consist of dimensionless parameters (M, Kn or Re), thermodynamic values (T_w, T_∞), gas properties and gas–surface molecular interaction parameters (s or v, D_e).

4.1. Shock wave structure

The shock wave structure is computed for various Mach numbers up to 10 reported in the literature. As discussed Section 1, due to the vibrational excitation the present results may be questionable in high Mach number cases. However, since the stagnation temperature in some experiments [7,29] is maintained such that the vibrational and chemical effects can be assumed to be negligible, the present comparison may be meaningful even in some high Mach number regime. The results of the inverse density thickness – one of

important factors characterizing the shock structure – are summarized in Fig. 4. In addition, a comparison with measurements of actual profiles of density by Alsmeyer [3] is shown in Fig. 5. The second-order accuracy was maintained in this computation. In all cases a grid of 500 points with $\Delta x = 0.4$ and the CFL number 0.5 are used. A steady-state solution was considered to be obtained when the rms norm for the density dropped below 10^{-7}. The general configuration of the shock inverse density thickness of the present solutions was shown to be in good agreement with experimental data and the DSMC result by Boyd et al. [8]. It should be mentioned that only thermal and rotational nonequilibrium effects are taken into account in the DSMC calculation. This may suggest that the present computational model is capable of calculating shock wave structures in the wide range of Mach number in good accuracy. However, it can be observed from Fig. 5 that there exists a deviation in actual density profiles, in particular, near the upstream state in the shock structure. This trend turned out to remain similar for other Mach numbers. The disagreement may be due to the omission of the term $\mathbf{Q} \cdot \nabla \mathbf{u}$ appearing in the constitutive relation of heat flux in the present formulation or the lack of the high temperature effects such as vibrational excitation and the temperature variation of specific heats in high Mach number cases. On the other hand, the Navier–Stokes theory yields the inverse widths much larger than those obtained by experiment and DSMC theory. The Navier–Stokes theory with Stokes' hypothesis gives the worst prediction. It may be concluded from this calculation that the bulk viscosity plays a vital role in nonequilibrium diatomic gas flows and, in particular, in the shock wave structure.

4.2. Two-dimensional hypersonic blunt body flow

The second problem considered in the present study is a hypersonic rarefied gas flow over a blunt body. The flow conditions are; $M = 5.48$, $Kn = 0.05$, $T_w = 293$ K, $T_\infty = 26.6$ K. As the first test case, a monatomic

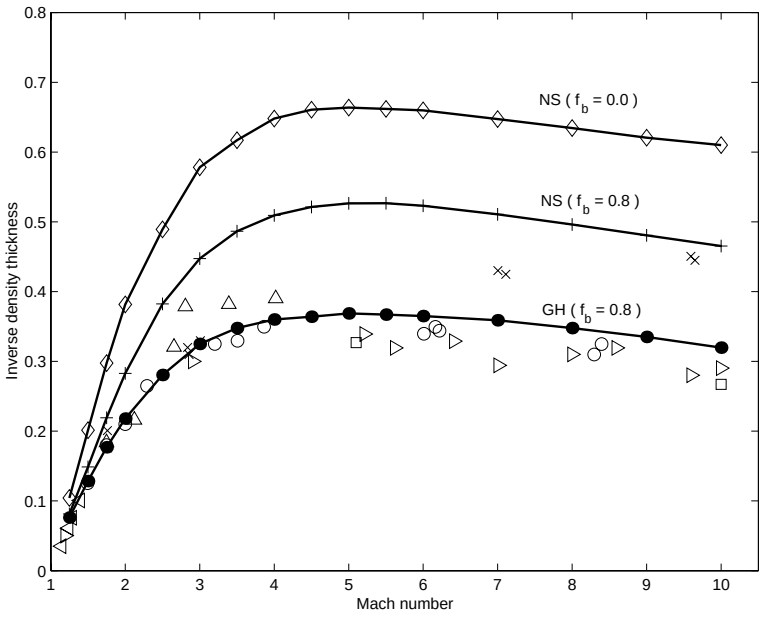

Fig. 4. Inverse shock density thickness for a diatomic gas (nitrogen, $s = 0.78$). The symbols are: (◁) by Greene and Hornig [21]; (△) by Linzer and Hornig [22]; (▷) by Camac [10]; (×) by Robben and Talbot [29]; and (○) by Alsmyer [3]. The squares (□) represent the results calculated by DSMC theory [8]. The line with the symbol (●) represents the value by the generalized hydrodynamic theory. The line with the symbol (+) represents the result by the Navier–Stokes theory. The line with the symbol (◇) represents the result by the Navier–Stokes theory with no bulk viscosity ($f_b = 0$).

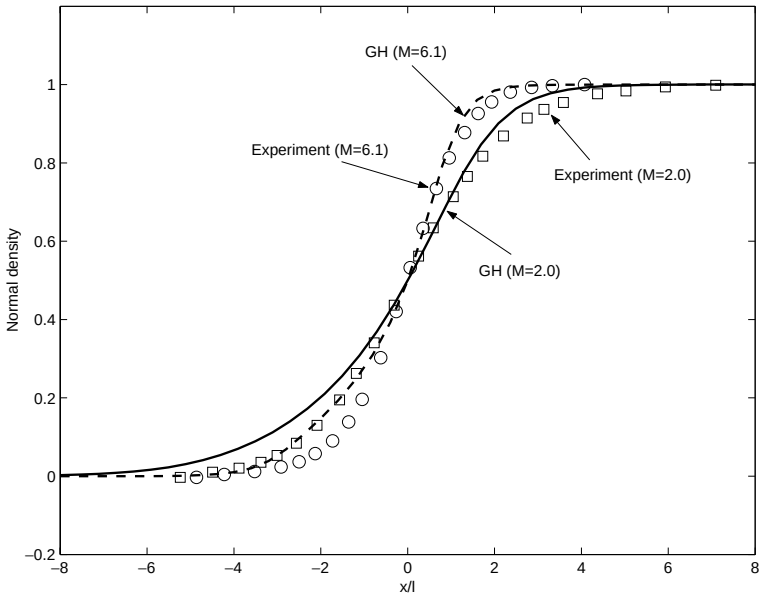

Fig. 5. Comparison of measured and computational normalized density profiles (nitrogen, $s = 0.78$). The symbols for experimental data obtained by Alsmyer [3] are: (□) for $M = 2.0$; and (○) for $M = 6.1$. The bold solid and dashed lines represent the results for $M = 2.0$, 6.1 by the generalized hydrodynamic theory ($f_b = 0.8$).

gas is considered; hard sphere molecule ($s = 0.5$ in the coefficient of viscosity, $c = 1.1908$). This case is included on the ground that a simple assessment of the present method can be made for the monatomic gas free from the complicated physical processes such as vibrational excitation. The computational domain is defined by a patch with a grid of 48×96 points and with near-wall adaptability. A gas–surface molecular interaction model for a monatomic gas is used, which depends on the pressure and temperature and provides the boundary values of temperature and velocity. The boundary condition at the outflow was specified by extrapolation. The slip condition on the wall was applied by defining the dual ghost cells, one for the inviscid part where the boundary values of velocity and temperature are specified, and another for the viscous part where the values at the wall are used. Owing to the large difference between the wall and free stream temperature a relatively small CFL number 0.1 is used. The first-order accuracy was maintained throughout the computational domain including the boundaries for simplicity.

The comparison of changes in conserved variables (normalized density and temperature) along the stagnation streamline is shown in Figs. 6 and 7. The R in the figures represents the characteristic length of the blunt body, which in the present case is the radius of a circular cylinder ($R = 20l_\infty$). The results calculated by the DSMC theory [34,35], the nonlinear model Boltzmann theory of Yang and Huang [38], and the Euler theory are considered for comparison with the results obtained by the present computational model. Only the DSMC result of hard sphere molecules by Vogenitz et al. [34] is shown in Fig. 6 since a recent DSMC result with the VHS collision model by Wetzel and Oertel [35] turns out to be almost the same. The flow structures consist of the bow shock and the stagnation region near the blunt body. As expected, all the results predict a rapid change of flow properties across the bow shock very close to the value given by the Rankine–Hugoniot relations. There exists, however, some discrepancy in the location and inner profiles of the bow shock between the continuum limit Euler solutions and non-continuum solutions (DSMC, nonlinear Boltzmann, and generalized hydrodynamics). The present computational model, nonlinear Boltzmann, and DSMC solutions yield results in close agreement.

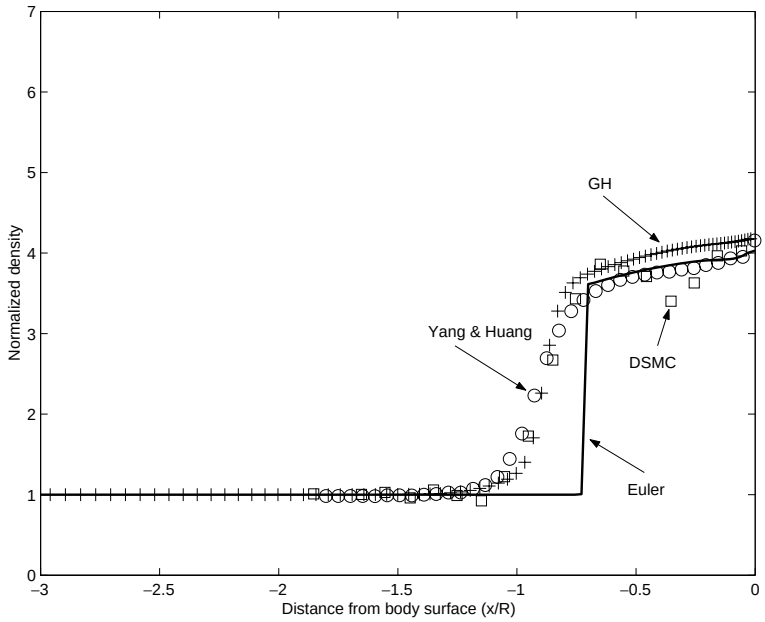

Fig. 6. Density distribution along stagnation streamline of a cylinder ($M = 5.48$, $Kn = 0.05$, hard sphere). The normalized density is defined as ρ/ρ_∞.

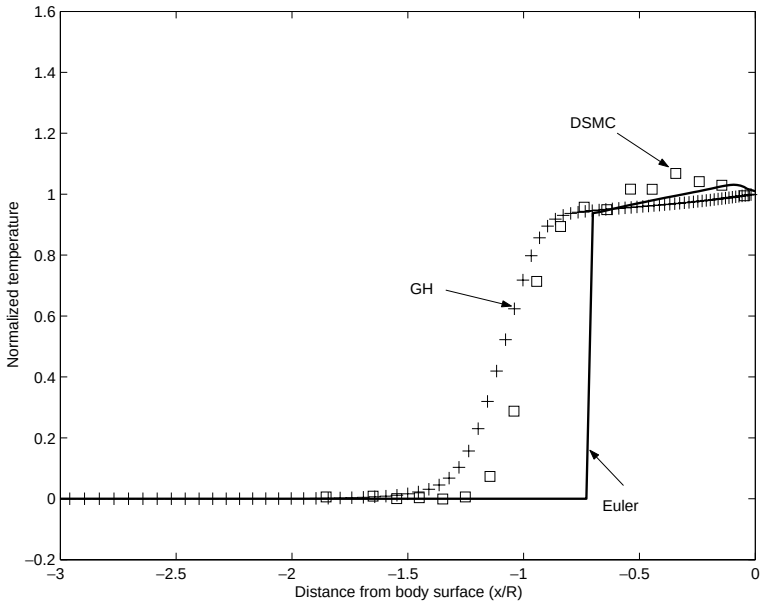

Fig. 7. Temperature distribution along stagnation streamline of a cylinder ($M = 5.48$, $Kn = 0.05$, hard sphere). The normalized temperature is defined as $(T - T_\infty)/(T_w - T_\infty)$.

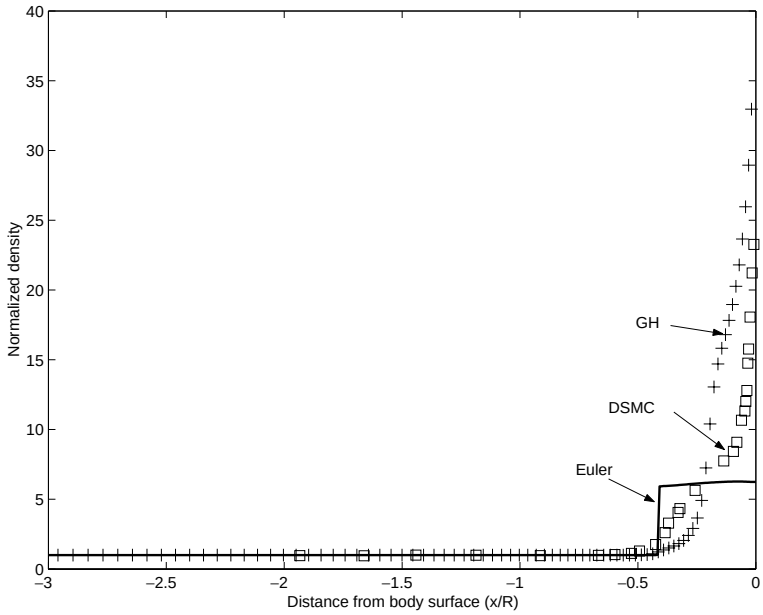

Fig. 8. Density distribution along stagnation streamline of a cylinder ($M = 20$, $Kn = 0.064$, nitrogen).

As the second test case, a more challenging problem – hypersonic nitrogen gas flow – is calculated by the new computational model. A gas–surface molecular interaction model for a diatomic gas represented by the (27) is used. The flow conditions are; $M = 20$, $Kn = 0.05$, $T_w = 291.6$ K, $T_\infty = 20$ K. Other conditions are exactly the same as the previous monatomic case. The comparison of normalized density changes along the stagnation streamline is shown in Fig. 8. Since the downstream temperature (about 1600 K) behind the shock with such high Mach number is beyond the vibrational excitation temperature, the comparison is limited to the DSMC result by Wu et al. [37] in which the vibrational effect is excluded from the calculation. In sharp contrast with the first case there exists a discrepancy in the general configuration of flow structures between the Euler solutions and the non-continuum solutions. The basic flow structure in the Euler theory remains the same as the first case – the bow shock and the stagnation region – but the structure in the non-continuum theory becomes the shock wave and boundary layer interaction type. It can be seen from Fig. 8 that for DSMC and generalized hydrodynamics results it is impossible to identify the line that separates the bow shock from the stagnation region or boundary layer near the wall. For the comparison of the present theory and DSMC, on the other hand, good agreement in qualitative aspect can be observed for the type of general flow structure and the density profile near the wall which is directly related to a gas particle pile-up. Some discrepancy appears, however, in the exact profiles within the shock wave and boundary layer interaction region. This may be attributed to, for example, the type of the energy interchange model, and the difference in implementing the molecular models. A validation study on these issues not only in the flow structure of conserved variables but also in the distribution of stress and heat flux near the wall will be required to clarify the source of the discrepancy in the future.

5. Concluding remarks

As a step toward developing computational models for nonequilibrium diatomic gas flows, Eu's generalized hydrodynamic equations of diatomic gases have been investigated. Eqs. (14)–(17) with the

boundary conditions (21) and (22) represent a complete set of the generalized hydrodynamic computational model for nonequilibrium diatomic gas flows. The model for diatomic gases reduces to the model for monatomic gases in the limit of vanishing bulk viscosity. In the new model the rotational nonequilibrium effect is taken into account by introducing excess normal stress associated with the bulk viscosity of the gas. The general properties of the constitutive equations are obtained through a simple mathematical analysis. With an iterative computational algorithm of the constitutive equations, numerical solutions for the multi-dimensional problem can be obtained. Numerical results of the shock wave structure and the rarefied hypersonic flow over a blunt body are presented. A qualitative agreement with experimental data and DSMC results is observed for the inverse shock density thickness and the general flow structure.

The high temperature gas effects such as vibrational excitation and dissociation were not included in the present formulation, since the emphasis was placed mainly on the translational and rotational modes of a diatomic gas and the development of computational models, starting from the Eu's generalized hydrodynamics. The inclusion of such effects is straightforward, but it will require considerable change of the present numerical algorithms. For example, the addition of the vibrational energy using the Landau-Teller rate model [4,33] is relatively simple, but the problem of solving the resulting equations becomes complicated, in particular, in numerical implementation. An extra source term is added to the conservation laws and the specific heats become temperature-dependent. In the shock structure problem the downstream states now depend on the upstream velocity and temperature. (In a calorically perfect gas, they depend only on the upstream Mach number.) The closed form of the Rankine-Hugoniot relation must be replaced by numerical solutions calculated by the iterative method.

In addition, numerical experiment was focused on the hypersonic rarefied gas flows because many experimental data and computational results using DSMC or higher-order equations are available. In the case of microscale gas flows, in addition to the lack of experimental data available, there remains a problem to develop a proper numerical method of the stiff generalized hydrodynamic equations for compressible low Mach number flows. Investigation of these problems using the Eu's generalized hydrodynamic computational models will be reported in the future work.

Acknowledgements

This work was supported by Korea Science and Engineering Foundation under Research Grant 1999-2-305-001-3. The author expresses his deep appreciation to Professor B.C. Eu in McGill University for his encouragement and advice and for reading the manuscript.

References

[1] M. Al-Ghoul, B.C. Eu, Generalized hydrodynamics and shock waves, Phys. Rev. E 56 (3) (1997) 2981–2992.
[2] M. Al-Ghoul, B.C. Eu, Generalized hydrodynamic theory of shock waves in rigid diatomic gases, Phys. Rev. E 64 (4) (2001) 6303–6315.
[3] H. Alsmyer, Density profiles in argon and nitrogen shock waves measured by the absorption of an electron beam, J. Fluid Mech. 74 (1976) 497–513.
[4] J.D. Anderson, Hypersonic and High Temperature Gas Dynamics, McGraw-Hill, New York, 1989.
[5] D.K. Bhattacharya, B.C. Eu, Nonlinear transport processes and fluid dynamics: Effects of thermoviscous coupling and nonlinear transport coefficients on plane Couette flow of Lennard–Jones fluids, Phys. Rev. A 35 (2) (1987) 821–836.
[6] G.A. Bird, Molecular Gas Dynamics and the Direct Simulation of Gas Flows, Clarendon Press, Oxford, England, 1994.
[7] I.D. Boyd, Analysis of rotational nonequilibrium in standing shock waves of nitrogen, AIAA J. 28 (11) (1990) 1997–1999.
[8] I.D. Boyd, G. Chen, G.V. Candler, Predicting failure of the continuum fluid equations in transitional hypersonic flows, Phys. Fluids 7 (1) (1995) 210–219.
[9] D. Burnett, The distribution of molecular velocities and the mean motion in a nonuniform gas, Proc. Lond. Math. Soc. 40 (1935) 382–435.

[10] M. Camac, in: J.H. de Leeuw (Ed.), Proceedings of the Fourth International Symposium on Rarefied Gas Dynamics, Adv. Appl. Mech. 1 (1965) 240.
[11] S. Chapman, T.G. Cowling, The Mathematical Theory of Nonuniform Gases, third ed., Cambridge Univ. Press, London, 1970.
[12] C.F. Curtiss, The classical Boltzmann equation of a gas of diatomic molecules, J. Chem. Phys. 75 (1981) 376–378.
[13] G. Emanuel, Bulk viscosity of a dilute polyatomic gas, Phys. Fluids A 2 (12) (1990) 2252–2254.
[14] B.C. Eu, R.E. Khayat, G.D. Billing, C. Nyeland, Nonlinear transport coefficients and plane Couette flow of a viscous, heat conducting gas between two plates at different temperatures, Can. J. Phys. 65 (1987) 1090–1103.
[15] B.C. Eu, Kinetic Theory and Irreversible Thermodynamics, Wiley, New York, 1992.
[16] B.C. Eu, Nonequilibrium Statistical Mechanics. Ensemble Method, Kluwer Academic Publishers, Dordrecht, 1998.
[17] B.C. Eu, Y.G. Ohr, Generalized hydrodynamics, bulk viscosity, and sound wave absorption and dispersion in dilute rigid molecular gases, Phys. Fluids 13 (3) (2001) 744–753.
[18] B.C. Eu, Generalized Thermodynamics: The Thermodynamics of Irreversible Processes and Generalized Hydrodynamis, Kluwer Academic Publishers, Dordrecht, 2002.
[19] M. Gad-el-Hak, The fluid mechanics of microdevices – the Freeman scholar lecture, J. Fluids Eng. 121 (1999) 5–33.
[20] H. Grad, On the kinetic theory of rarefied gases, Commun. Pure Appl. Math. 2 (1949) 331–407.
[21] E.F. Greene, D.F. Hornig, The shape and thickness of shock fronts in argon, hydrogen, nitrogen, and oxygen, J. Chem. Phys. 21 (4) (1953) 617–624.
[22] M. Linzer, D.F. Hornig, Structure of shock fronts in argon and nitrogen, Phys. Fluids 6 (12) (1963) 1661–1668.
[23] F.E. Lumpkin III, D.R. Chapman, C. Park, A new rotational relaxation model for use in hypersonic computational fluid dynamics, Technical Paper 89–1737, AIAA Press, Washington, DC, 1989.
[24] J.C. Maxwell, On the Dynamical Theory of Gases, Collected Works of J.C. Maxwell, Cambridge University Press, London, 1927, pp. 26–78 (Philos. Trans. Roy. Soc. Lond. 159 (1867) 49).
[25] I. Müller, T. Ruggeri, Extended Thermodynamics, Springer, New York, 1993.
[26] R.S. Myong, Thermodynamically consistent hydrodynamic computational models for high-Knudsen-number gas flows, Phys. Fluids 11 (9) (1999) 2788–2802.
[27] R.S. Myong, A computational method for Eu's generalized hydrodynamic equations of rarefied and microscale gas dynamics, J. Comput. Phys. 168 (2001) 47–72.
[28] R.S. Myong, Velocity-slip Effect in Low-speed Microscale Gas Flows, AIAA Paper 2001-3076, AIAA Press, Washington, DC, 2001.
[29] F. Robben, L. Talbot, Measurement of shock wave thickness by the electron beam fluorescence method, Phys. Fluids 9 (4) (1966) 633–643.
[30] J.M. Reese, L.C. Woods, F.J.P. Thivet, S.M. Candel, A second order description of shock structure, J. Comput. Phys. 117 (1995) 240–250.
[31] B. van Leer, Flux-vector splitting for the Euler equations, Technical Report ICASE 82-30, NASA Langley Research Center, 1982.
[32] B. van Leer, On the relation between the upwind-differencing schemes of Godunov, Enguist–Osher and Roe, SIAM J. Sci. Stat. Comput. 5 (1) (1985) 1–20.
[33] W.G. Vincenti, C.H. Kruger, Introduction to Physical Gas Dynamics, Wiley, New York, 1967.
[34] F.W. Vogenitz, G.A. Bird, J.E. Broadwell, H. Rungaldier, Theoretical and experimental study of rarefied supersonic flows about several simple shapes, AIAA J. 6 (12) (1968) 2388–2394.
[35] W. Wetzel, H. Oertel, Direct Monte Carlo simulations of hypersonic flows past blunt bodies, Progr. Astronaut. Aeronaut. 118 (1989) 432–446.
[36] F.M. White, Viscous Fluid Flow, McGraw-Hill, 1974.
[37] J.S. Wu, K.C. Tseng, C.H. Kuo, Application of local mesh refinement in the DSMC method, in: Rarefied Gas Dynamics: 22nd International Symposium, AIP Conference Proceedings, vol. 585, 2001, pp. 417–425.
[38] J.Y. Yang, J.C. Huang, Rarefied flow computations using nonlinear model Boltzmann equations, J. Comput. Phys. 120 (1995) 323–339.
[39] K.Y. Yun, R.K. Agarwal, R. Balakrishnan, Augmented Burnett and Bhatnagar–Gross–Burnett equations for hypersonic flow, J. Thermophys. Heat Transfer 12 (3) (1998) 328–335.